Journal of Materials Chemistry C

ROYAL SOCIETY OF CHEMISTRY

PAPER

View Article Online
View Journal | View Issue

Cite this: J. Mater. Chem. C, 2020, 8, 3226

Elegant design of carbon nanotube foams with double continuous structure for metamaterials in a broad frequency range

Zhenmin Jiao, [ab] Dagmar R. D'hooge, [cd] Ludwig Cardon*[b] and Jun Qiu *[ae]

Received 16th November 2019,
Accepted 24th January 2020

DOI: 10.1039/c9tc06291b

rsc.li/materials-c

Carbon nanotube (CNT) foams with negative permittivity and permeability are successfully prepared by chemical vapor deposition (CVD) and post-treatment. A double negative metamaterial in the 1–1000 MHz frequency range with double continuous structure results by effectively compounding the CNT foam with a polymer material, *i.e.* epoxy or nanosilver silicone resin. The negative permeability is specifically attributed to the three-dimensional CNT interactions as clear from the study of the relation of the material microstructure and the macroscopic measurements. Compared to CNT foam/epoxy composites, CNT foam/nanosilver/silicone composites have a lower permeability but a more excellent electrical conductivity or permittivity. It is also shown that the carbon source time during CVD and post-pressurization can be adjusted to allow for both negative permittivity and permeability. This contribution highlights a convenient method to obtain a metamaterial in a much larger frequency range (*ca.* 1 to 1000 MHz) than the state-of-the-art. It thus supports the expansion of the application range of metamaterials and simplifies their preparation, which is of great significance for the wider use of these materials.

1 Introduction

The need for high-quality energy absorbing materials and structures (EAMS) has created an upsurge of interest in the materials science and engineering research field. Interesting is a so-called double continuous phase composite (DCPC), a nomenclature introduced by Clarke[1] to define a multicomponent material in which a reinforcing body and matrix are intertwined and continuously distributed in a three-dimensional space. Due to its special structure, DCPC has many advantages, such as low density, high specific modulus, high specific strength, fatigue resistance, and heat resistance. A low thermal expansion coefficient, the eliminated stress concentration at the interface, the smooth transition of stiffness, the reduction of the amount of applied materials, and the strong bonding between printed materials are DCPC characteristics that cannot be easily obtained with conventional composites.[2] DCPCs are therefore widely used in modern engineering, *e.g.* for the development of thermal protective sweating materials for aerospace vehicles, high-temperature self-lubricating composite materials, and high-performance ceramic-based metal composites.[3–5]

DCPCs have attracted wide attention due to their special structure and were first developed by Japanese scholars from Nabeya and Bridgestone who jointly developed a cast iron-based porous ceramic composite, which was named Breathnite.[6] After the DCPC discovery most attention has been paid to the design of the mechanical properties.[7–9] More recent research has also highlighted the potential of foam, hence, lightweight, metal/polymer double-phase composites.[10,11] They are higher order multi-phase materials with each phase interspersing and entangling in the internal three-dimensional space through a continuous topology. They also induce isotropic macroscopic properties, contributing to the improvement of the overall performance.[12–14] These new more lightweight materials have already been widely used, *e.g.* for friction and wear parts under special conditions, and electronic packaging, ballistic, and damping materials.[15,16]

The polymer is typically an epoxy resin, which has the advantages of high mechanical strength,[17,18] strong adhesion to metal and non-metal surfaces,[19] good corrosion resistance,[20] dimensional stability,[21] and low cost. Alternatively, a nano-silver/silicone resin combines conductive silver nanoparticles[22–24] with a matrix silicone resin to form a conductive path to achieve an electrically conductive connection of the material. Attention has

[a] School of Materials Science and Engineering, Tongji University, Shanghai 201804, P. R. China. E-mail: qiujun@tongji.edu.cn; Tel: +86 15900983488
[b] Centre for Polymer and Material Technologies, Department of Materials, Textiles and Chemical Engineering, Ghent University, Technologiepark 130, Zwijnaarde, Ghent 9052, Belgium. E-mail: ludwig.cardon@ugent.be; Tel: +32 93310391
[c] Laboratory for Chemical Technology, Department of Materials, Textiles and Chemical Engineering, Ghent University, Technologiepark 125, Zwijnaarde, Ghent 9052, Belgium
[d] Centre for Textile Science and Engineering, Department of Materials, Textiles and Chemical Engineering, Ghent University, Technologiepark 70A, Zwijnaarde, Ghent 9052, Belgium
[e] Key Laboratory of Advanced Civil Engineering Materials (Tongji University), Education of Ministry, Shanghai 201804, P. R. China

also been focused on the inclusion of carbon nanotubes (CNTs), which are one-dimensional quantum materials with a special tubular structure that have excellent properties such as low density, high strength and large specific surface area.[25–32] Upon their introduction at the surface of the matrix of the composite, this not only improves the wettability between the interfaces, but they also embed in the filling phase, which greatly enhances the bonding strength between the matrix and the filling phase, thereby improving forced compatibility and providing synergy.[33]

In the last decade, so-called double negative metamaterials with (unconventional) both negative permittivity and negative permeability have been investigated, as they induce uncommon behavior such as a reverse Doppler effect, reverse Cherenkov radiation, and a negative refractive index.[34] Therefore, they are widely used in sub-wavelength imaging, "invisibility", filters, planar lens design, and antenna performance improvement.[35–37]

Initially most researchers focused on structural design of metamaterials[38–46] and limited work has been done to explore negative permittivity[47–49] and/or negative permeability from the perspective of natural materials. Sui *et al.*[50] prepared a carbon nanofiber/polyetherimide (CNF/PEI) composite film with a thickness ranging from 20 to 30 mm, which exhibites a negative permittivity in the frequency range of 10^{-2} to 10^{7} Hz. Moreau *et al.*[51] demonstrated a simple method for fabricating metamaterials by randomly adsorbing chemically synthesized silver nanotubes onto a nanoscale thick polymer spacer layer of a gold film. Guo *et al.*[52] found that polypropylene-based elastomers containing CNF have a negative permittivity. Shi *et al.*[53] placed an iron network in porous alumina through the impregnation–reduction process, and negative permittivity and negative permeability appeared in the high frequency range for the composite with an iron content of 20–27 m%. The composition and microstructure of the material are controlled, with the double negative material behavior likely in the metal magnetic particles. Hence, it is possible to explore the composition of metal-based double negative materials, instead of relying on the construction of complex artificial structures to achieve double negative performance. Different from metal magnetic particle composite metamaterials, Yao *et al.*[54] realized a multi-walled CNT/polyaniline (PANI) composite, which exhibits double negative performance again in the high frequency range, with breakage of the polymer composite also leading to double negative performance. Furthermore, Kou *et al.*[55] realized the double negative performance of a CNF/polypyrrole composite in the high frequency range.

It thus worthwhile to further investigate whether the control of CNT incorporation is relevant to achieve a wider range of double negative character. A challenge is here still to prepare DCPC metamaterials with double negative performance, hence, joint negative permittivities and permeabilities, in a broad frequency range (*e.g.* 1 to 1000 MHz) in a more convenient and efficient way. In the present contribution, CNT/foam nickel composites, *i.e.* so-called CNT foams, are manufactured that are successful in this respect, which creates a significant step forward regarding the application potential.

Foam nickel is used as a skeleton to support and transfer stress, with CNTs grown on the surface of the nickel foam by chemical vapor deposition (CVD). In order to expand the scope of these foams – specifically their strength to enable DCPC features – they are also combined with epoxy resin and nano-silver/silicone polymer resin. It is shown that compared to the CNT foam/epoxy composite, the CNT foam/nano-silver/silicone resin composite has a less negative permittivity but a more excellent electrical conductivity. Due to their special foam-based double continuous structure, the designed structures are a new type of lightweight damping materials, which are expected to play a role as sound-absorbing metamaterials.[56,57] Moreover, since the compressive properties and conductivity of the CNT foams allow pressure response characteristics they are also applicable to chemically resistant vapor sensors and ultrasensitive pressure sensors.

2 Experimental

2.1 Chemicals

Nickel foam (purity of nickel 99.8%, porosity 95%, PPI110, thickness 3 mm) was purchased from Suzhou Yulong Technology Co., Ltd, China. Distilled water, hydrochloric acid, sodium hydroxide, and anhydrous ethanol were purchased from Sinopharm Chemical Reagent Co., Ltd China. High-purity nitrogen was purchased from Shanghai Dumao Purification Gas Co., Ltd. Conductive silver glue with component A and component B was from Nanjing Helite Adhesive Co., Ltd. Epoxy resin was purchased from Huntsman Chemical Trading Co., Ltd. 622 epoxy resin thinner was from Shanghai Demao Chemical Co., Ltd. Epoxy resin curing agent was from Huntsman Chemical Trading Co., Ltd. The epoxy resin de-foaming agent was from Shanghai Demao Chemical Co., Ltd. All chemicals were used as-received without any further treatment.

2.2 Preparation of CNT foam starting from nickel foam

The nickel foam was cut into 2 cm × 1 cm rectangular strips and treated with 5% hydrochloric acid, and 5% sodium hydroxide and sodium carbonate mixed solution for 20 min. It was then washed with distilled water and placed in the middle of a quartz boat with tweezers, with the quartz boat placed in the middle of the reaction zone of the tubular sintering furnace. The sealing valve was at one point closed to connect the devices, the rotameter was opened, the temperature program 30 °C (80 min)–400 °C (60 min)–400 °C (60 min)–700 °C (15–30 min)–700 °C (106 min)–210 °C of the furnace was set, and the time of the carbon source ethanol was controlled (*e.g.* 15–30 min). By simultaneously allowing entry of the protective gas nitrogen, controlling the flow rate at 10 ml min^{-1}, waiting until the end of the set procedure and cooling to room temperature, the carbon nanotube (CNT) foam resulted. Finally, the sample was taken out, post-treated and tested.

2.3 Preparation of modified nickel foams and their use as foam/polymer composites

Epoxy resin, curing agent, thinner, and resin de-foaming agent are uniformly mixed at room temperature in a plastic cup in a certain mass proportion (*e.g.* 6.22/3.57/1.00/0.30). A nickel or

CNT foam is immersed in the prepared epoxy resin solution for 3 minutes, and is cured in a surface dish for 48 hours starting at room temperature to obtain a nickel or CNT foam/epoxy composite.

The commercial nanosilver silicone resin contains two components, named component A and component B, and the nanosilver silicone resin solution is arranged according to a mass ratio A : B of 10 : 1. The CNT foam is immersed in the prepared nano silver silicone resin solution for 2 min, and then moved to a surface dish and cured starting at room temperature for 72 hours. A nanosilver silicone resin/CNT foam composite is thus obtained.

2.4 Characterization

Scanning electron microscopy (SEM) images were taken on a Quanta FEG 250 field emission scanning electron microscope. Transmission electron microscopy was performed using a JEOL JEM-2010 (HT) electron microscope. The permittivity properties were investigated using an LCR meter (Agilent, E4991A) equipped with a dielectric detector (Agilent, 16453A) at a frequency of 10^6 to 10^9 Hz at room temperature. The sample was a wafer with a diameter of 20 mm and a thickness of 2–4 mm. The wafer was coated with conductive silver paste on the top and bottom surface and dried in a vacuum at 80 °C for 4 h in order to form two electrodes before testing. The permeability properties were investigated using an LCR meter (Agilent, E4991A) equipped with a permeability detector (Agilent, 164 54A) at a frequency of 10^6 to 10^9 Hz at room temperature. The sample was a toroidal core structure wafer with an inner diameter of 5 mm, and an outer diameter of 15 mm, and a thickness of 4–7 mm. The resistivity was tested using an electrochemical workstation CHI660E in the frequency range 1–10^5 Hz. The sample used to test the resistivity was the same as the sample for the dielectric property test, which was a wafer with a diameter of 20 mm and thickness of 2–4 mm coated with conductive silver paste on the top and bottom surface to form two electrodes for the test. Upon testing, the test electrode and the opposite electrode were clamped separately at the two ends of the sample.

3 Results and discussion

3.1 Permittivity and permeability of nickel foam *vs.* CNT foam

Fig. 1 shows the frequency dependencies of the permittivity and permeability of nickel foam and CNT foams with three carbon source times. It can be seen in Fig. 1(a) (black solid symbols; left axis) and Fig. 1(b) (enlargement of the purple oval in Fig. 1(a)) that the permittivity of nickel foam is negative in the full frequency range. When the frequency is 1×10^8 Hz, the permittivity value is -10^5, and as the frequency increases, the permittivity shows an increasing trend until the curve starts to stabilize near a frequency of 4×10^8 Hz. This can be explained by dielectric relaxation as accessible with the Drude model,[58] which implies that the electric field changes are faster compared to the frequency increase so that the internal electrons cannot keep up with the change in the applied electric field, which ultimately leads to the absolute value of the negative permittivity being reduced.[59] When the frequency is 1×10^9 Hz, the permittivity value of nickel foam is about -7×10^2 (see Fig. 1(b)).

Compared with the nickel foam, the negative permittivity of the CNT foams (coloured solid symbols in Fig. 1; three carbon source times: 15 min (red), 20 min (blue), and 30 min (green)) is significantly reduced, but still exhibits negative values in the full frequency range. The growth of carbon nanotubes destroys the three-dimensional network structure of the nickel foam itself, and then decreases the carrier concentration in the nickel network, which results in a decrease of the absolute value of permittivity. More importantly, it can be seen that the permittivity of the CNT foams depends on the carbon source time, with the most negative values for 20 minutes (blue solid symbols) (when the frequency is 1×10^8 Hz (Fig. 1b), the permittivity value is -6.2×10^3 (blue solid symbol)), followed by the 15 min CNT foam (-3.1×10^3, red solid symbol), and the 30 min CNT foam (-2.2×10^3, green solid symbol).

As shown in Fig. 1(a) (hollow symbols; right axis), the permeability of the nickel foam and the CNT foam of 15 min and 30 min is positive in the full frequency range and the values are substantially the same. If the frequency is 10^8 Hz, the

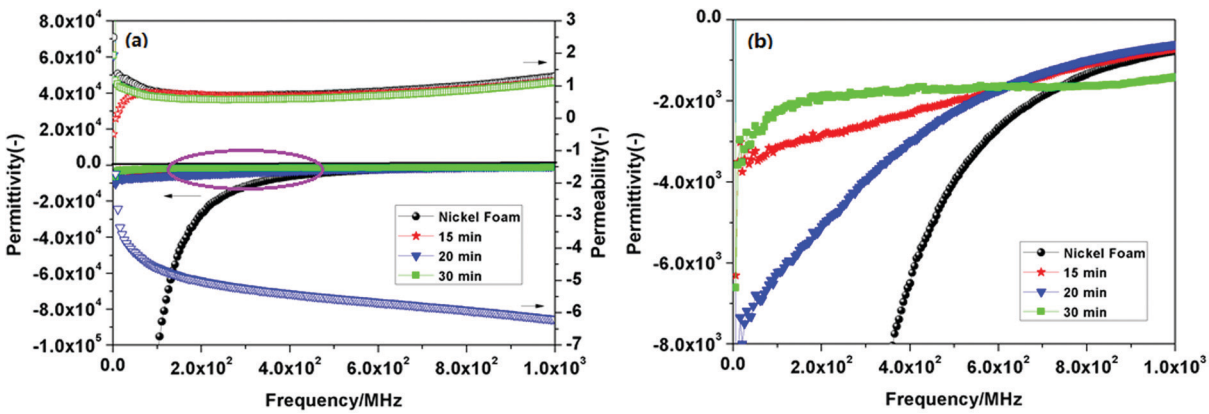

Fig. 1 (a) Permittivity (solid symbols) and permeability (hollow symbols) of nickel foam (black) and carbon nanotube (CNT) foam for 3 carbon source access times (15 min red, 20 min blue, and 30 min green) and (b) an enlargement of the permittivities for the CNT foam oval in (a); for the 20 min CNT foam a double negative metamaterial is obtained (no pressurization) for a large frequency range covering both low and high frequencies.

permeability values of the nickel foam and the 15 min CNT foam are 0.8, while the 30 min CNT foam has a similar value of 0.6. If the frequency is 10^9 Hz, the values are 1.2, 1.1, and 1.1, respectively. In contrast, the permeability of the CNT foam with a carbon source time of 20 min (hollow blue symbols in Fig. 1(a)) is significantly different, with the permeability now negative over the entire frequency range, and as the frequency increases the curve displays a downward trend. Hence, with 20 minutes an intrinsic metamaterial is obtained with double negative properties in the full frequency range (both negative blue solid and hollow symbols).

The relation of the material structure and double negative performance has been explored by sample morphological analysis. SEM images of the CNT foam with a carbon source time of 20 min, hence, for a double negative metamaterial, are shown in Fig. 2. It follows that CNTs are grown on the surface of the nickel foam, and these CNTs are strongly entangled with each other, forming the desired three-dimensional network structure. If the carbon source is introduced for 15 minutes, however, the amount of CNTs grown on the surface of the nickel foam is still small, as shown in Fig. 3(a). Also sporadic thin carbon tubes and other carbon impurities can be produced on the surface of the nickel foam, as shown in Fig. 3(b) and (c) (cases of longer reaction times). Hence, an optimum reaction condition is expected to ensure the best of the two effects so that well-defined multi-walled CNTs are prepared, as shown in the TEM image with a carbon source time of 20 min in Fig. 3(d).

Only if the carbon source is introduced for 20 minutes (Fig. 3(b)) are the carbon impurities significantly reduced, the CNT content increased, and the diameter of the CNTs significantly increased, forming an entangled network structure. If the carbon source is further increased to 30 minutes (Fig. 3(c)), the carbon impurities begin to increase again, and occupy most of the space. This is because the diameter of the CNTs is determined by the size of the nickel nanoparticles. Generally, at a higher reaction temperature, the nickel nanoparticles are melted and thus in a semi-liquid state, which can lead to aggregation into larger nanoparticles, resulting in larger diameter CNTs. At the same time, some of the larger nickel nanoparticles decompose into smaller nanoparticles, resulting in smaller CNT formation. After 30 minutes, more nickel particles are consumed, more impurities are formed, and the diameter of the growing carbon tubes is on a net basis largely altered, and there is no obvious intertwining network structure anymore.

Negative permittivity is generated by the plasma oscillation of delocalized electrons in a conductive network.[39] The negative permeability is derived from abundantly present conductive closed loops. Therefore, only the 20 min CNT foam exhibits double negative performance.

It can be derived from Fig. 4 (hollow symbols) that after (manually) applying a certain pressure to the CNT foams negative permeability can be obtained for all carbon access times. The CNT foams of 15 min and 30 min have a positive permeability before pressure (red and green hollow symbols in Fig. 4), and change from positive to negative after pressing (dark cyan and dark yellow hollow symbols). The permeability of the CNT foam of 20 min reaction time is also more negative (hollow blue *vs.* magenta symbols in Fig. 4). The reason is that the CNT foam parts which are not originally joined together are now entangled with each other due to the reduction of the distance with pressure so that a large number of conductive loops would be formed, further

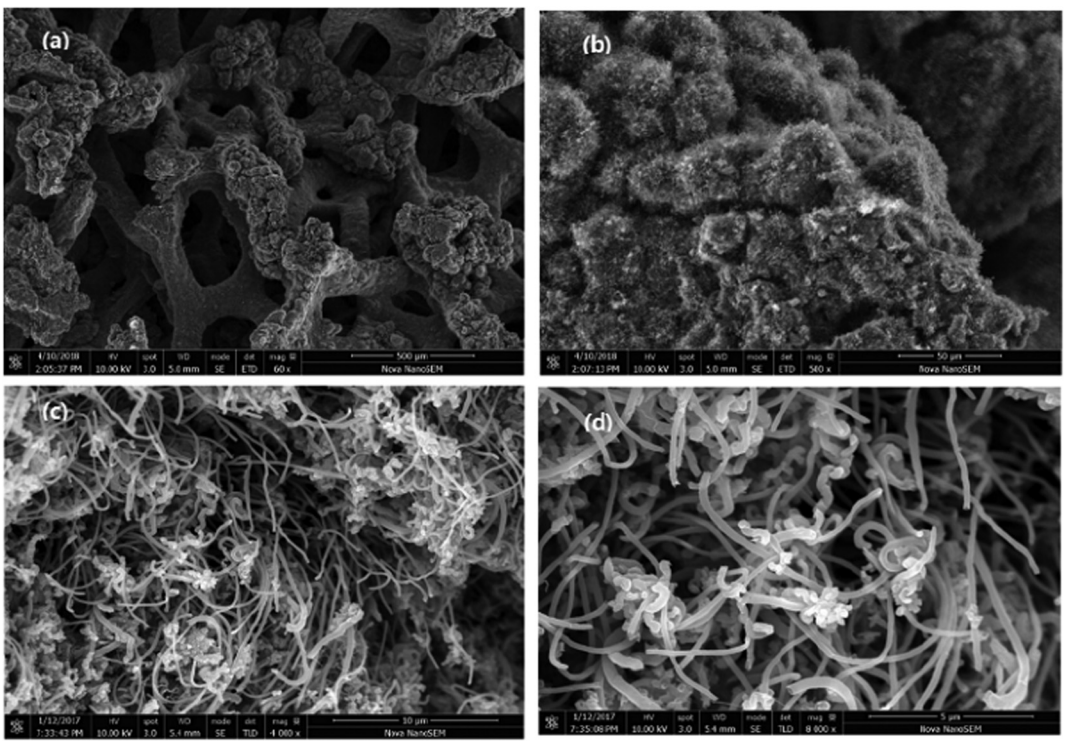

Fig. 2 Scanning electron micrograph of the carbon nanotube foam with a carbon source access time of 20 min that leads to a double negative metamaterial (Fig. 1; blue symbols) (a) 500 μm, (b) 50 μm, (c) 10 μm, and (d) 5 μm. Comparison with other carbon access times in Fig. 3.

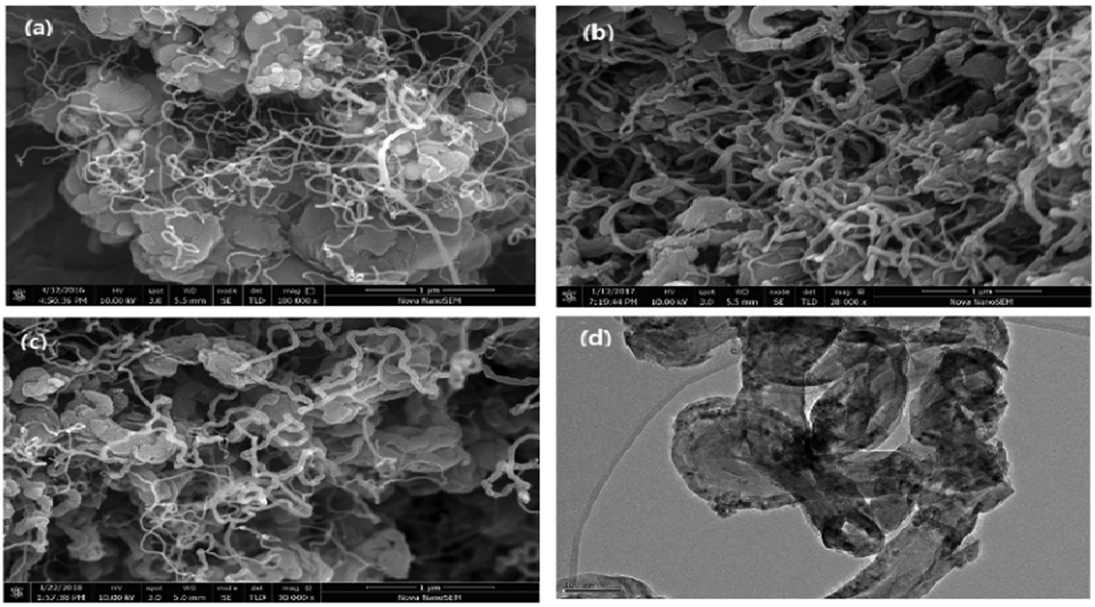

Fig. 3 Scanning electron micrograph of the carbon tube foam with carbon source access times (a) 15 min, (b) 20 min, and (c) 30 min; 1 μm. (d) Transmission electron microscope picture (with carbon source access time 20 min): 100 nm; only for 20 min do we see the desired double negative behaviour with an entangled 3D network with lesser importance of impurities.

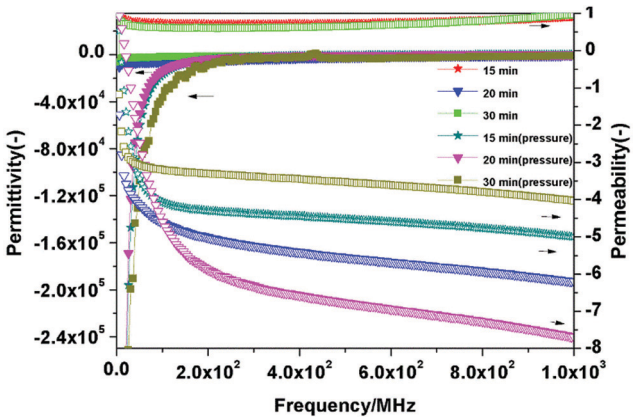

Fig. 4 Relevance of pressurization to tune the permittivity (solid symbols) and permeability (hollow symbols) of the carbon nanotube foam with varying carbon source access times (15 min red + dark cyan, 20 min blue + magenta, and 30 min green + dark yellow).

highlighting the mechanism of the permeability as introduced above. The sum of the induced electric field and polarization electric field exceeds the original electric field, resulting in the occurrence of a negative permittivity. The large number of conductive loops formed after pressurization generates a strong diamagnetic response, resulting in a negative permeability. Hence, the CNT foams can be produced into intrinsic metamaterials from natural materials by applying pressurization.

3.2 Permittivity and permeability of CNT foam/polymer composites

It can be seen in Fig. 5(a) and (b) that the permittivity of the nickel/epoxy composite foam (no CNT foam yet for clarity; yellow solid symbols) is negative and the permeability is positive (yellow hollow symbols) in the whole frequency range. The results show that the addition of epoxy resin has a limited effect on the dielectric properties of the nickel foam. This phenomenon is also observed from the permittivity and permeability values of the CNT foam (blue symbols) and CNT foam/epoxy composites (pink symbols). The permittivity and permeability of the two are as good as coincident, verifying that the epoxy resin has good wave permeability and does not – at least to a first approximation – affect the dielectric properties of the material itself.

Hence, we obtained a DPCP with CNT foam as the reinforcement and epoxy resin as the matrix. The reason why the epoxy resin is added is that the CNT foam itself is not high in structural strength and is not easy to use in an engineering structure. The composite of the CNT foam and epoxy resin can thus be employed to prepare a DCPC, which can effectively expand the applications of the CNT foam. The DCPC material requires that the reinforcement and the matrix are intertwined and uniformly distributed in a three-dimensional space. As CNTs have a large specific surface area, the wettability of the surface of the nickel foam can be enhanced, so that the resin is more fully impregnated with the nickel foam. Not only is the wettability between the interfaces improved, but also the CNTs are embedded in the filling phase, forming good interfacial contact and greatly enhancing the bonding strength between the matrix and the filling phase.

As shown in Fig. 5(c), the CNT/epoxy resin composite has the highest resistivity, and the value is between 70 and 80 $\Omega\ cm^{-1}$. Foam nickel/epoxy resin composites and CNT foam/epoxy composites have lower resistivity, with the former stable at around 3 $\Omega\ cm^{-1}$, and the latter stable at around 1 $\Omega\ cm^{-1}$. The resistivity data show

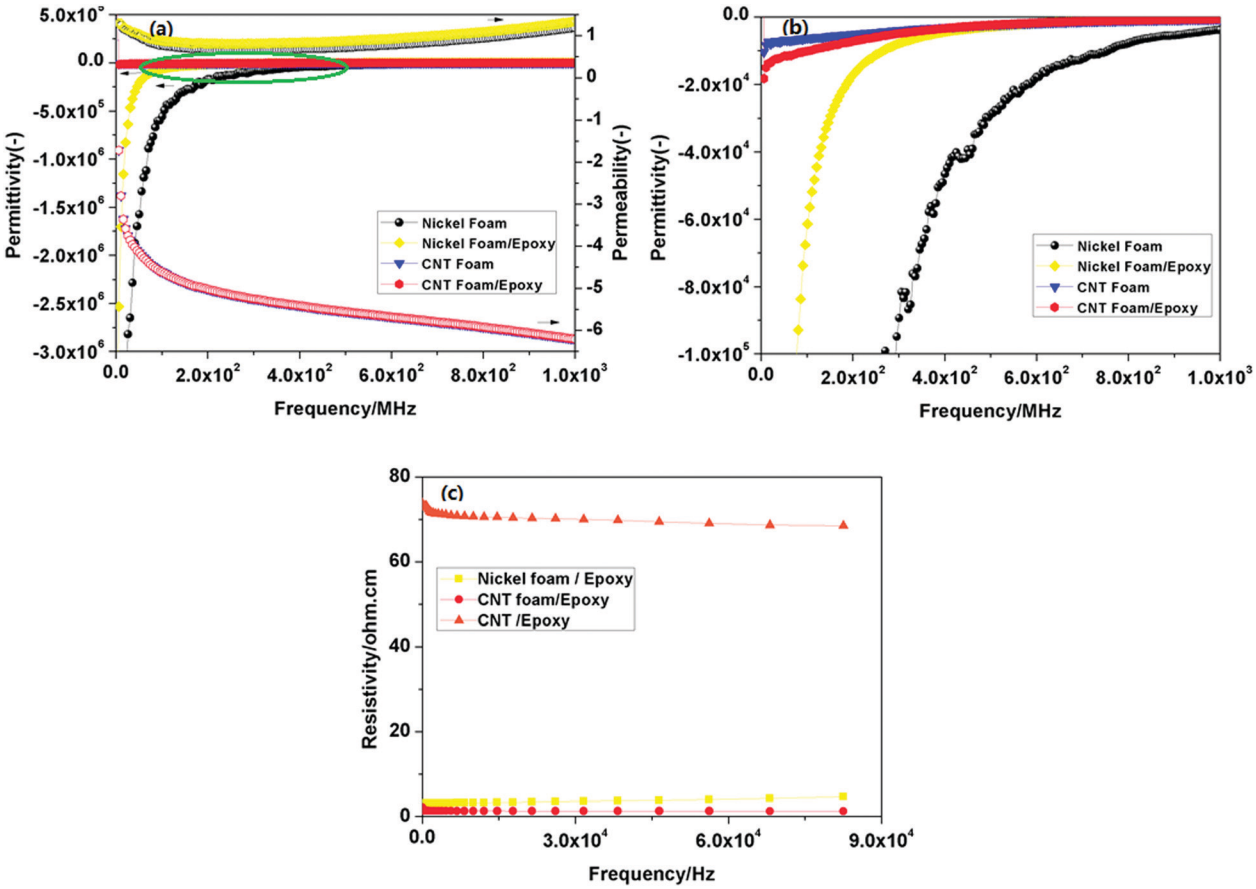

Fig. 5 (a) Permittivity (solid symbols) and permeability (hollow symbols) of the nickel foam (black), nickel foam/epoxy resin composite (yellow), carbon nanotube (CNT) foam (blue; 20 min from Fig. 1; a carbon source time of 20 min; no pressurization), and carbon nanotube foam/epoxy resin composite (pink); (b) an enlargement (green oval) of the permittivities; and (c) resistivities involving epoxy resin; by producing a composite with epoxy and CNT foam the double negative behavior can be maintained and a DPCP results.

the excellent electrical conductivity of the foam nickel/epoxy resin and CNT foam/epoxy composite due to its double continuous structure. Compared with the nickel foam/epoxy composite, the CNT foam composite plays a significant role because it is an intrinsic metamaterial, and with the presence of nickel the electrical resistivity is reduced by an

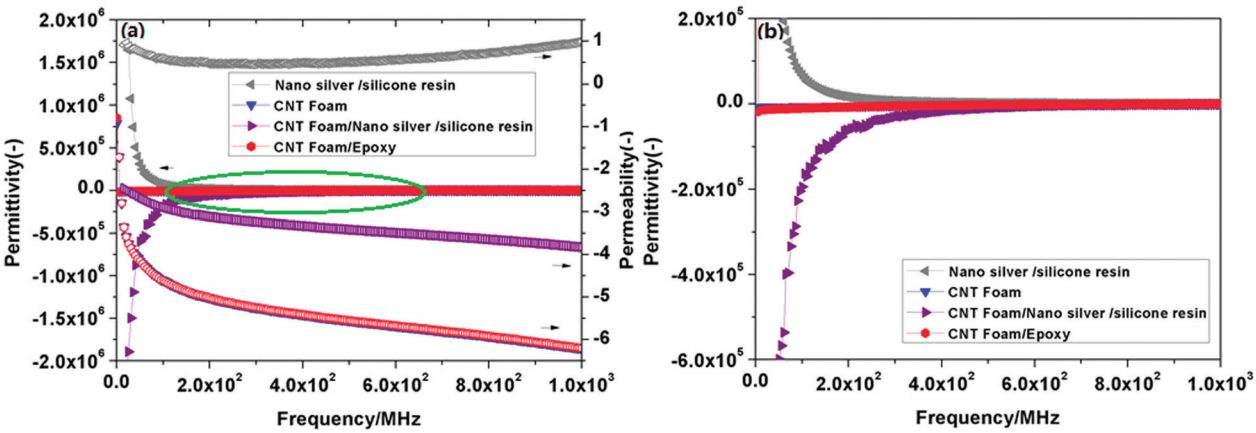

Fig. 6 (a) Permittivity (solid symbols) and permeability (hollow symbols) of the nanosilver/silicone resin (gray; undesired positive values; SEM image in Fig. 7), carbon nanotube (CNT) foam (blue; 20 min; from Fig. 1; a carbon source time of 20 min; no pressurization), CNT foam/epoxy resin (pink; from Fig. 5), and carbon nanotube foam/nanosilver/silicone resin (purple). The latter leads to a double negative metamaterial with in particular much lower permittivities compared the CNT foam/epoxy resin. The permeabilities are however less negative as deducible from the SEM images in Fig. 8. (b) Enlargements of permittivities (green oval).

order of magnitude, comparable to that of discontinuous phase composites.

As shown in Fig. 6, the permittivity and permeability of the alternative nanosilver silicone resin are positive in the full frequency range (grey solid and hollow symbols), and the permittivity gradually becomes stable with increasing frequency. When the frequency is 10^9 Hz, the value of the permittivity is 1.1×10^3 and the basic value fluctuates around 1 in the full frequency range. Fig. 7 shows the corresponding SEM microstructure. It follows that the surface does not have any holes or three-dimensional network structure. The generation of negative permittivity and negative permeability requires a certain amount of conductive network formation, consistent with the discussion of Fig. 2 and 3. The microstructures in Fig. 7 thus give a reason why the permittivity and permeability of the nanosilver/silicone resin are positive in the full frequency range.

Fig. 6 additionally reconfirms that that CNT foam (blue symbols) and CNT foam/epoxy (pink symbols) composites, as studied above, lead to negative permittivities and permeabilities in the full frequency range. Compared with CNT foam/epoxy composites, the permittivity of the CNT foam/nanosilver/silicone resin composite (purple solid symbols) is significantly reduced,

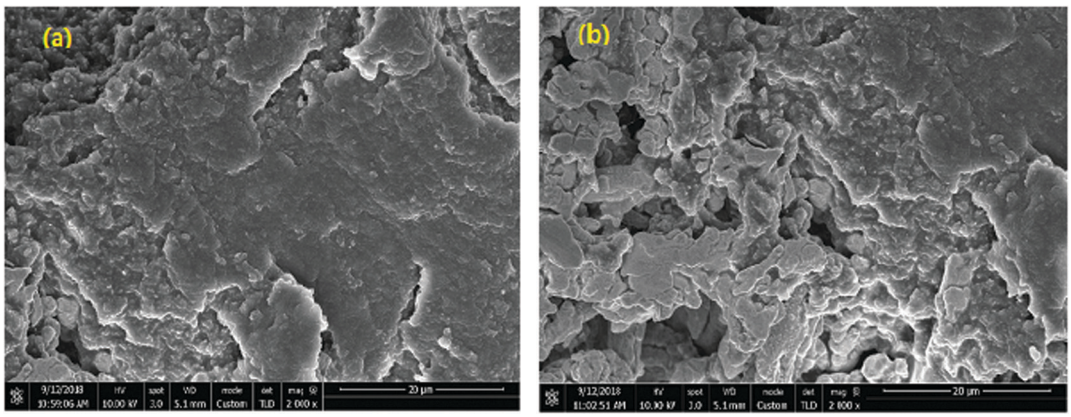

Fig. 7 SEM photo of the nanosilver/silicone resin (related to the grey line in Fig. 6) displaying positive permittivity and permeability, as there is no elegant network formation (a) 20 μm and (b) 20 μm.

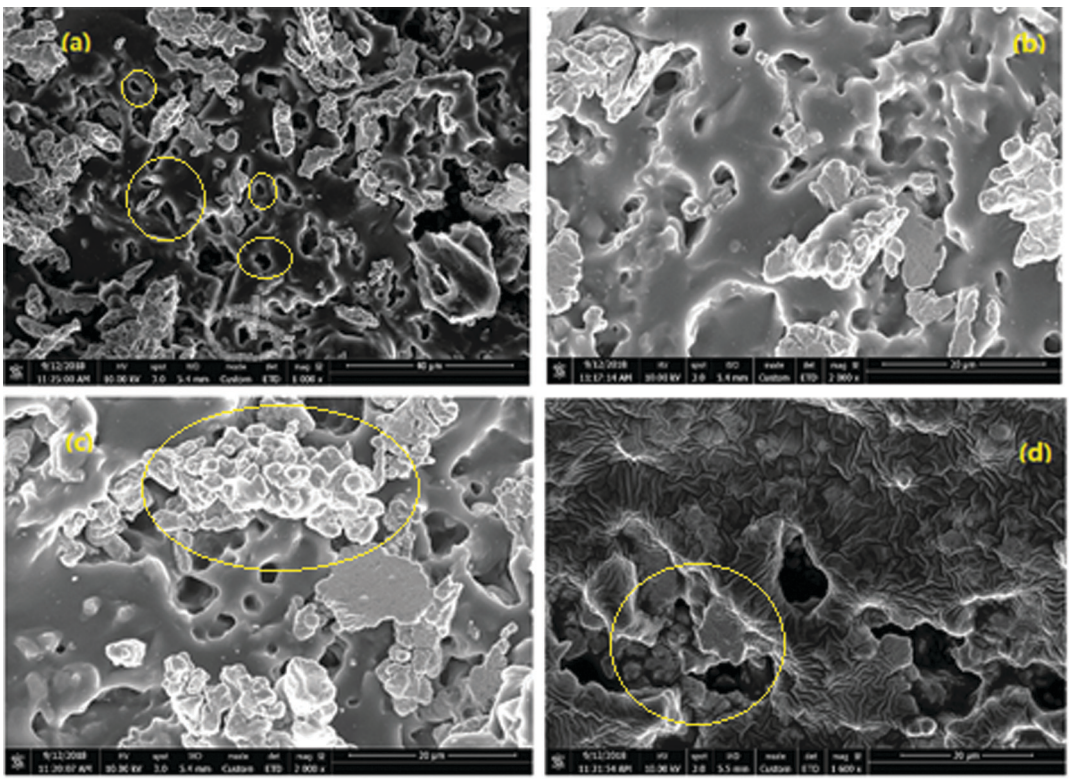

Fig. 8 SEM images of the carbon nanotube foam/nanosilver/silicone resin composite (related to the purple symbols in Fig. 6) (a) 40 μm, (b) 20 μm, (c) 20 μm, and (d) 20 μm.

with the values decreased by two orders of magnitude. This indicates that the addition of nano-silver effectively increases the number of free electrons, which enhances the plasma oscillation of the delocalized electrons in the conductive network and facilitates the reduction of the dielectric constant. The permeability (purple open symbols) is however less negative, as can also be understood from the SEM images in Fig. 8.

It can be seen in Fig. 8(a) that the CNT foam/nanosilver/silicone resin composite exhibits the desired structure of a double continuous phase. Porous holes appear on the surface, and some pores and holes are even connected to each other. The two phases in the double continuous composites are uniformly continuous in three-dimensional space, so that the stress is uniformly transmitted in all directions, hindering a crack from expanding in a certain direction. However, from Fig. 8(b)–(d) it follows that also blockage by the resin part occurs, and a large amount of nano-silver silicone resin is attached to the surface of the CNT foam. The overlapping three-dimensional network structure is therefore hindered, and the number of closed conductive loops in the system is reduced, which suppresses the decrease of the permeability. It should however be stressed that on an overall basis a well-defined metamaterial is still obtained. Furthermore, the material itself is much lighter than other metal-based metamaterials because of the special porous structure of the bi-continuous phase.

4 Conclusions

Intrinsic metamaterials based on CNT foam are successfully prepared by chemical vapor deposition (CVD). It is shown that the carbon source time during CVD needs to be designed to allow for both negative permittivity and permeability or that pressurization needs to be applied. Two DCPCs are reported by respectively combining the CNT foam with epoxy and nano silver/silicone resin, while maintaining double negative performance in a much broader frequency range compared to the state-of-the art. The use of nickel foam to prepare the CNT foams allows us to obtain high electrical resistivity comparable to that of discontinuous phase composites.

The SEM results show that for the optimized conditions the composite phases interweave and entangle each other in a three-dimensional space, and exhibit isotropic properties on a macroscopic scale. Because of its special double continuous structure not only is the wettability between the interfaces improved but also the bonding strength between the matrix and the filling phase is greatly enhanced.

Compared to the CNT foam/epoxy resin composite, the carbon nanotube foam/nano silver/silicone resin composite material has a less decreased permeability but a more excellent electrical conductivity. The addition of silver nanoparticles effectively increases the number of free electrons in the system, which enhances the plasma oscillation of the delocalized electrons in the conductive network and positively promotes the decrease of the permittivity.

It is expected that the developed new lightweight materials – with large frequency range applicability and a more straightforward manufacturing method – will not only continue to play a role in electromagnetic metamaterials, but also display application potential in the field of noise reduction.

Conflicts of interest

There are no conflicts to declare.

Acknowledgements

This work was supported by the Natural Science Foundation of Shanghai (16ZR1446200) and we also appreciate funding from the China Scholarship Council (grant 201806260112) for the joint-PhD study at Ghent university.

Notes and references

1 D. R. Clarke, *J. Am. Ceram. Soc.*, 1992, **75**, 739–758.
2 N. Dukhan, N. Rayess and J. Hadley, *Mech. Mater.*, 2010, **42**, 134–141.
3 M. Bahraini, E. Schlenther, J. Kriegesmann, T. Graule and J. Kuebler, *Composites, Part A*, 2010, **41**, 1511–1515.
4 S. Q. Niu, J. Zhu and J. L. Ouyang, *Tribology*, 1995, **15**, 324–332.
5 W. G. Li, Y. Y. Chen and T. H. Wu, *J. Chin. Chem. Soc.*, 2010, **38**, 1468–1472.
6 Y. Takagi, T. Kikuchi and C. Katayama, *J. Synchrotron Radiat.*, 1998, **5**, 854–856.
7 Y. Liu, D. L. Duan, J. X. Wang, S. Hou and S. Li, *Chin. J. Mater. Res.*, 2016, **30**, 909–913.
8 B. P. Xie, S. L. Yan, X. He, C. Li and X. X. Yang, *Acta Mater. Compositae Sin.*, 2017, **34**, 1325–1333.
9 N. N. Ni, Y. F. Wen, D. L. He, X. S. Yi, M. C. Guo and Y. H. Xu, *J. Mater. Eng.*, 2015, **43**, 90–101.
10 Y. Yu, X. Wu and P. Xu, *Adv. Mater. Res.*, 2011, **146–147**, 318–322.
11 Z. Y. Wang and L. S. Yang, *Dev. Appl. Mater.*, 2004, **3**, 38–40.
12 B. P. Xie, S. L. Yan, H. Xu, C. Li and X. X. Yang, *Acta Mater. Compositae Sin.*, 2017, **34**, 1325–1333.
13 W. H. Xie, H. T. Du and S. C. Li, *Acta Mater. Compositae Sin.*, 2011, **28**, 103–108.
14 A. P. Tian, W. Yu and D. J. Li, *Acta Mater. Compositae Sin.*, 2013, **30**, 74–81.
15 Y. Liu, D. L. Duan, J. X. Wang, S. H. Hou and S. Li, *Chin. J. Mater. Res.*, 2017, **30**(12), 909–913.
16 G. Gorrasi, V. Bugatti, C. Milone, E. Mastronardo, E. Piperopoulos, L. Iemmo and A. Di Bartolomeo, *Composites, Part B*, 2018, **135**, 149–154.
17 J. X. Zhang, Y. X. Liang, X. Wang, H. J. Zhou, S. Y. Li, J. Zhang, Y. Feng, N. Lu, Q. Wang and Z. Guo, *Adv. Compos. Hybrid Mater.*, 2018, **1**, 300–309.
18 L. Guadagno, B. De Vivo, A. Di Bartolomeo, P. Lamberti, A. Sorrentino, V. Tucci, L. Vertuccio and V. Vittoria, *Carbon N. Y.*, 2011, **49**, 1919–1930.
19 X. Yang, Y. Guo, X. Luo, N. Zheng, T. Ma, J. Tan, C. Li, Q. Zhang and J. Gu, *Compos. Sci. Technol.*, 2018, **164**, 59–64.

20 D. Sun, J. An, G. Wu and J. Yang, *J. Mater. Chem. A*, 2015, **3**, 4435–4444.
21 C. Liang, P. Song, H. Gu, C. Ma, Y. Guo, H. Zhang, X. Xu, Q. Zhang and J. Gu, *Composites, Part A*, 2017, **102**, 126–136.
22 Y. Oh, K. Y. Chun, E. Lee, Y. J. Kim and S. Baik, *J. Mater. Chem.*, 2010, **20**, 3579–3582.
23 H. Jiang, K. S. Moon, Y. Li and C. P. Wong, *Chem. Mater.*, 2006, **18**, 2969–2973.
24 Y. Li, K. S. Moon and C. P. Wong, *Science*, 2005, **308**, 1419–1420.
25 B. W. Kim, S. Pfeifer, S. H. Park and P. R. Bandaru, *Mater. Res. Soc. Symp. Proc.*, 2011, **1312**, 281–286.
26 N. Grossiord, J. Loos, O. Regev and C. E. Koning, *Chem. Mater.*, 2006, **18**, 1089–1099.
27 X. Guan, G. Zheng, K. Dai, C. Liu, X. Yan, C. Shen and Z. Guo, *ACS Appl. Mater. Interfaces*, 2016, **8**, 14150–14159.
28 H. Gu, H. Zhang, C. Ma, X. Xu, Y. Wang, Z. Wang, R. Wei, H. Liu, C. Liu, Q. Shao, X. Mai and Z. Guo, *Carbon N. Y.*, 2019, **142**, 131–140.
29 C. Lin, L. Hu, C. Cheng, K. Sun, X. Guo, Q. Shao, J. Li, N. Wang and Z. Guo, *Electrochim. Acta*, 2018, **260**, 65–72.
30 Z. Li, B. Wang, X. Qin, Y. Wang, C. Liu, Q. Shao, N. Wang, J. Zhang, Z. Wang, C. Shen and Z. Guo, *ACS Sustainable Chem. Eng.*, 2018, **6**, 13747–13755.
31 Q. Luo, H. Ma, Q. Hou, Y. Li, J. Ren, X. Dai, Z. Yao, Y. Zhou, L. Xiang, H. Du, H. He, N. Wang, K. Jiang, H. Lin, H. Zhang and Z. Guo, *Adv. Funct. Mater.*, 2018, **28**, 1–8.
32 K. Zhang, G. H. Li, L. M. Feng, N. Wang, J. Guo, K. Sun, K. X. Yu, J. B. Zeng, T. Li, Z. Guo and M. Wang, *J. Mater. Chem. C*, 2017, **5**, 9359–9369.
33 L. Dong, F. Hou, Y. Li, L. Wang, H. Gao and Y. Tang, *Composites, Part A*, 2014, **56**, 248–255.
34 Y. Yao and X. P. Zhao, *J. Appl. Phys.*, 2007, **101**, 124904.
35 A. Ali and Z. Hu, *Microwaves, Antennas*, 2007, **2**, 561–566.
36 A. J. Hoffman, L. Alekseyev, S. S. Howard, K. J. Franz, D. Wasserman, V. A. Podolskiy, E. E. Narimanov, D. L. Sivco and C. Gmachl, *Nat. Mater.*, 2007, **6**, 946–950.
37 Q. Wu and W. Park, *Appl. Phys. Lett.*, 2008, **92**, 90–93.
38 V. G. Veselago, *Sov. Phys. Uspekhi*, 1968, **10**(4), 509.
39 J. B. Pendry, A. J. Holden, D. J. Robbins and W. J. Stewart, *IEEE Trans. Microwave Theory Tech.*, 1999, **47**, 2075–2084.
40 D. R. Smith and N. Kroll, *Phys. Rev. Lett.*, 2000, **85**, 2933–2936.
41 R. A. Shelby, D. R. Smith and S. Schultz, *Science*, 2001, **292**, 77–79.
42 J. Zhou, L. Zhang, G. Tuttle, T. Koschny and C. M. Soukoulis, *Phys. Rev. B: Condens. Matter Mater. Phys.*, 2006, **73**, 1–4.
43 S. Xiao, V. P. Drachev, A. V. Kildishev, X. Ni, U. K. Chettiar, H. K. Yuan and V. M. Shalaev, *Nature*, 2010, **466**, 735–738.
44 G. He, R. X. Wu, Y. Poo and P. Chen, *J. Appl. Phys.*, 2010, **107**, 093522.
45 H. Tao, J. J. Amsden, A. C. Strikwerda, K. Fan, D. L. Kaplan, X. Zhang, R. D. Avertit and F. G. Omenetto, *Adv. Mater.*, 2010, **22**, 3527–3531.
46 W. M. Zhu, A. Q. Liu, X. M. Zhang, D. P. Tsai, T. Bourouina, J. H. Teng, X. H. Zhang, H. C. Guo, H. Tanoto, T. Mei, G. Q. Lo and D. L. Kwong, *Adv. Mater.*, 2011, **23**, 1792–1796.
47 C. Cheng, R. Fan, Z. Wang, Q. Shao, X. Guo, P. Xie, Y. Yin, Y. Zhang, L. An, Y. Lei, J. E. Ryu, A. Shankar and Z. Guo, *Carbon N. Y.*, 2017, **125**, 103–112.
48 K. Sun, P. Xie, Z. Wang, T. Su, Q. Shao, J. E. Ryu, X. Zhang, J. Guo, A. Shankar, J. Li, R. Fan, D. Cao and Z. Guo, *Polymer*, 2017, **125**, 50–57.
49 P. Xie, Z. Wang, Z. Zhang, R. Fan, C. Cheng, H. Liu, Y. Liu, T. Li, C. Yan, N. Wang and Z. Guo, *J. Mater. Chem. C*, 2018, **6**, 5239–5249.
50 G. Sui, B. Li, G. Bratzel, L. Baker, W. H. Zhong and X. P. Yang, *Soft Matter*, 2009, **5**, 3593–3598.
51 A. Moreau, C. Ciracì, J. J. Mock, D. R. Smith, R. T. Hill, A. Chilkoti, Q. Wang and B. J. Wiley, *Nature*, 2012, **492**, 86–89.
52 J. Zhu, S. Wei, J. Ryu and Z. Guo, *J. Phys. Chem. C*, 2011, **115**, 13215–13222.
53 Z. C. Shi, R. H. Fan, K. L. Yan, K. Sun, M. Zhang, C. G. Wang, X. F. Liu and X. H. Zhang, *Adv. Funct. Mater.*, 2013, **23**, 4123–4132.
54 X. Yao, X. Kou and J. Qiu, *Carbon N. Y.*, 2016, **107**, 261–267.
55 X. Kou, X. Yao and J. Qiu, *J. Polym. Sci., Part B: Polym. Phys.*, 2017, **55**, 1724–1729.
56 M. Yang and P. Sheng, *Annu. Rev. Mater. Res.*, 2017, **47**, 83–114.
57 J. P. Groby, C. Lagarrigue, B. Brouard, O. Dazel, V. Tournat and B. Nennig, *J. Acoust. Soc. Am.*, 2014, **136**, 1139–1148.
58 S. T. Chui and L. Hu, *Phys. Rev. B: Condens. Matter Mater. Phys.*, 2002, **65**, 1–6.
59 X. Yao, X. Kou and J. Qiu, *Org. Electron.*, 2016, **38**, 55–60.

